Journal of Cerebral Blood Flow & Metabolism (2013) 33, 1115–1126

www.jcbfm.com

ORIGINAL ARTICLE

Mitochondrial calcium uptake capacity modulates neocortical excitability

Basavaraju G Sanganahalli[1,2,3], Peter Herman[1,2,3], Fahmeed Hyder[1,2,3,4] and Sridhar S Kannurpatti[5]

Local calcium (Ca^{2+}) changes regulate central nervous system metabolism and communication integrated by subcellular processes including mitochondrial Ca^{2+} uptake. Mitochondria take up Ca^{2+} through the calcium uniporter (mCU) aided by cytoplasmic microdomains of high Ca^{2+}. Known only *in vitro*, the *in vivo* impact of mCU activity may reveal Ca^{2+}-mediated roles of mitochondria in brain signaling and metabolism. From *in vitro* studies of mitochondrial Ca^{2+} sequestration and cycling in various cell types of the central nervous system, we evaluated ranges of spontaneous and activity-induced Ca^{2+} distributions in multiple subcellular compartments *in vivo*. We hypothesized that inhibiting (or enhancing) mCU activity would attenuate (or augment) cortical neuronal activity as well as activity-induced hemodynamic responses in an overall cytoplasmic and mitochondrial Ca^{2+}-dependent manner. Spontaneous and sensory-evoked cortical activities were measured by extracellular electrophysiology complemented with dynamic mapping of blood oxygen level dependence and cerebral blood flow. Calcium uniporter activity was inhibited and enhanced pharmacologically, and its impact on the multimodal measures were analyzed in an integrated manner. Ru360, an mCU inhibitor, reduced all stimulus-evoked responses, whereas Kaempferol, an mCU enhancer, augmented all evoked responses. Collectively, the results confirm aforementioned hypotheses and support the Ca^{2+} uptake-mediated integrative role of *in vivo* mitochondria on neocortical activity.

Journal of Cerebral Blood Flow & Metabolism (2013) **33,** 1115–1126; doi:10.1038/jcbfm.2013.61; published online 17 April 2013

Keywords: aging; brain injury; BOLD; calcium uniporter; CBF; mitochondria

INTRODUCTION

Local control of calcium (Ca^{2+}) in subcellular compartments influences central nervous system metabolism and communication. Ca^{2+} waves propagate along individual cells and through network of connected cells of neuronal and glial types integrated by various cytoplasmic Ca^{2+} buffering proteins and subcellular organelles such as the mitochondria.[1] Mitochondria take up Ca^{2+} primarily through a uniporter (mCU) mechanism buffering some of it and efflux the excess free Ca^{2+}. Novel biophysical approaches in the past few decades have revealed the integrating role of mitochondrial Ca^{2+} cycling in neural metabolism[2,3] and signaling.[4–8] Characterized mostly *in vitro*, the impact of mitochondrial Ca^{2+} cycling activity on brain function *in vivo* is still largely unexplored. As both deficient[9,10] and hyperactive mitochondrial metabolism[11,12] are implicated in neuropathology, a systems-level assessment of mitochondrial functional impact on central nervous system responses, possibly through translatable measures, is important.

From *in vitro* studies of Ca^{2+} in slices and various cell types of the central nervous system,[2,4,5,7,8,13–25] we evaluated spontaneous and evoked activity state-dependent Ca^{2+} ranges in multiple compartments *in vivo* consisting of the extracellular space as well as microdomains of cytoplasm and mitochondria (Figure 1). We hypothesized that diminished mCU activity signifying deficient mitochondrial function via decreased Ca^{2+} cycling will decrease mitochondrial Ca^{2+} with unchanged to minimally decreased overall cytoplasmic Ca^{2+} (overall = cytoplasmic + microdomains) (Figures 1B and 1E), leading to reduced oxidative metabolism, electrical activity, and hemodynamic response. Whereas enhanced mCU activity signifying hyperactive mitochondrial function via increased Ca^{2+} cycling will increase overall cytoplasmic Ca^{2+} and mitochondrial Ca^{2+} (Figures 1C and 1F), leading to augmented oxidative metabolism, electrical activity, and hemodynamic response. We tested the hypotheses using extracellular electrical activity of neuronal populations, blood oxygen level dependent (BOLD) and cerebral blood flow (CBF) measures in intact anesthetized rats. Calcium uniporter was inhibited using Ru360.[6,26] Ru360 with actions specific to mCU activity is known to always reduce mitochondrial Ca^{2+} uptake in various cell types,[6,27–29] leading to decreased or unchanged overall cytoplasmic Ca^{2+} transients during stimulation[13,30] and in some cases increased overall cytoplasmic Ca^{2+}.[6] Calcium uniporter activity was enhanced using Kaempferol, a compound known to increase mitochondrial and overall cytoplasmic Ca^{2+} levels.[31–34] Calcium uniporter inhibition with Ru360 treatment diminished the stimulus-evoked neuronal activity, BOLD, and CBF responses whereas enhanced mCU activity with Kaempferol treatment, depending on the dose, augmented most stimulus-evoked measures. Collectively, the results confirm our hypotheses and

[1]Department of Diagnostic Radiology, Yale University School of Medicine, New Haven, Connecticut, USA; [2]Magnetic Resonance Research Center (MRRC), Yale University School of Medicine, New Haven, Connecticut, USA; [3]Core Center for Quantitative Neuroscience with Magnetic Resonance (QNMR), Yale University School of Medicine, New Haven, Connecticut, USA; [4]Department of Biomedical Engineering, Yale University School of Medicine, New Haven, Connecticut, USA and [5]Department of Radiology, UMDNJ-New Jersey Medical School, Newark, New Jersey, USA. Correspondence: Dr SS Kannurpatti, Department of Radiology, UMDNJ-New Jersey Medical School, ADMC Bldg 5, Suite 575, Bergen Street, Newark, New Jersey 07103, USA.
E-mail: kannursr@umdnj.edu
This work was supported by grants from the American Heart Association 0930132N (SK) and National Institute of Health P30NS052519 (FH).
Received 1 January 2013; revised 14 March 2013; accepted 15 March 2013; published online 17 April 2013

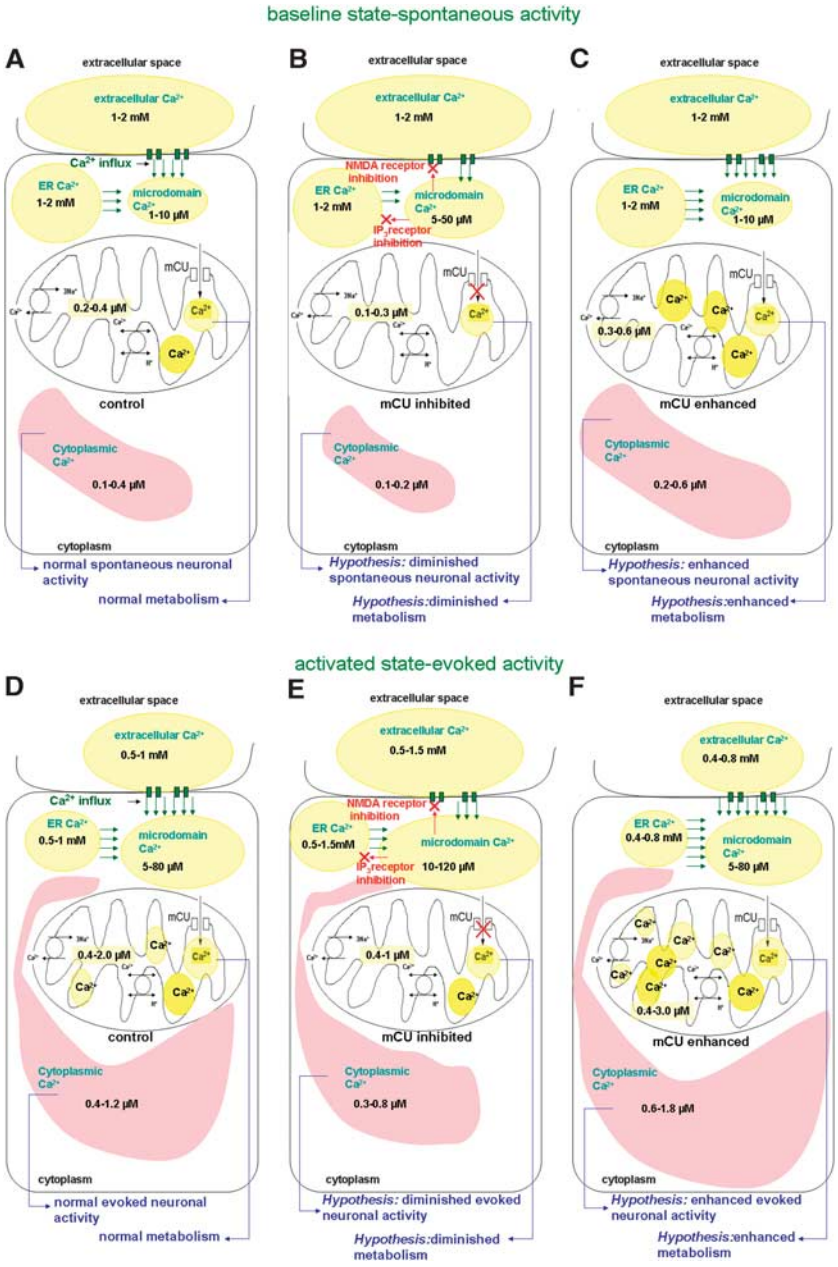

Figure 1. Multicompartment distribution of free Ca^{2+} hypothesized in the brain *in vivo* during the baseline conditions (**A**–**C**) and evoked neural activity conditions (**D**–**F**) based on *in vitro* literature on Ca^{2+} measurements from neurons, glia, and brain slices.[2,4,5,7,8,13–25] (**D**) During normal physiologic conditions, evoked brain activity can decrease extracellular and endoplasmic reticular Ca^{2+} ranges, and increase cytoplasmic and mitochondria Ca^{2+} ranges. (**E**) During mCU inhibition, evoked activity can lead to a relatively smaller decrease in extracellular and endoplasmic reticular (ER) Ca^{2+} ranges and smaller increase in cytoplasmic and mitochondrial Ca^{2+} ranges. Accumulating microdomain Ca^{2+} may inhibit plasma membrane glutamate receptors and mobilization from the ER stores resulting in reduced cytoplasmic Ca^{2+}. This leads to the hypothesis that diminished mitochondrial Ca^{2+} influx capacity will reduce neocortical excitability, metabolism, and hemodynamic response. (**F**) During mCU enhancement, evoked activity can lead to relatively larger decreases in extracellular and ER Ca^{2+} ranges and relatively larger increases in cytoplasmic and mitochondrial Ca^{2+} ranges. Augmented clearance of Ca^{2+} in the microdomains by mitochondria may delay the Ca^{2+}-mediated N-methyl-D-aspartate receptor desensitization resulting in larger cytoplasmic Ca^{2+} ranges. This leads to the hypothesis that enhanced mitochondrial Ca^{2+} influx capacity will increase neocortical excitability, metabolism, and hemodynamic response.

suggest that mitochondrial Ca^{2+} uptake capacity alters neocortical neuronal activity and hemodynamic responses.

MATERIALS AND METHODS

Surgical Preparation

Experimental procedures were carried out in accordance with protocols approved by the Institutional Animal Care and Use Committees of the University of Medicine and Dentistry of New Jersey and Yale University, in agreement with the National Institutes of Health Guide for the Care and Use of Laboratory Animals and ARRIVE guidelines. Sprague–Dawley rats (Male; 250 to 300 g; $n = 37$) were anesthetized with urethane (1.3 g/kg, intraperitoneal) for the functional laser Doppler imaging (fLDI) and functional magnetic resonance imaging (fMRI) experiments, and α-chloralose (40 mg/kg per hour, intravenous) for the electrophysiology experiments. Animals in the electrophysiology group were surgically

prepared under 2% isoflurane and switched to α-chloralose during the recording phase.

Choice of urethane or α-chloralose anesthesia was made considering the hypothesis to be tested, experimental design, and physiologic variables of interest. Depending upon their suitability, urethane, isoflurane, meditomedine, or α-chloralose anesthesia are commonly used anesthetics for fMRI and electrophysiological studies. Isoflurane was not preferred in the present study because of its dose-related effects on the neurovascular coupling[35] and undesired alteration of cortical glutamatergic transmission. As cellular calcium signaling was central to our hypothesis of mitochondrial action, meditomedine was avoided as it could interfere with the L- and P-type calcium channel functions known to facilitate calcium-activated potassium channels in a voltage-gated manner. α-chloralose is the most commonly used anesthetic in rodent neuroimaging and physiology experiments from early studies showing that this agent preserved the robust hemodynamic and metabolic coupling to sensory stimulation.[36,37] Urethane, another widely used anesthetic, minimally affects cardiovascular, respiratory, and spinal reflexes, providing long-term stability and balanced actions on multiple neurotransmitter receptors.[38] Hence, α-chloralose or urethane was suitably used with urethane preferred for the relatively longer fLDI and fMRI experiments. As similar evoked potentials and neuronal-hemodynamic coupling exist between α-chloralose and urethane anesthesia,[39] there were no major anesthetic confounds affecting the results.

The animal's core temperature was monitored and maintained at $37 \pm 0.5^{\circ}C$ with a rectal probe and homeothermic blankets. Rats were endotracheally intubated and mechanically ventilated. Partial pressure of the end-tidal carbon dioxide levels was maintained between 32 to 36 mm Hg by appropriate ventilatory adjustments. The left femoral artery was catheterized using PE50 tubing for measurement of mean arterial blood pressure (MABP), while the left femoral vein was catheterized for infusion of drugs. Mean arterial blood pressure was monitored in all experiments and blood gases were measured in the electrophysiological and fMRI experiments.

For electrical recording measurements, the scalp was retracted and a burr hole was made over the contralateral somatosensory forelimb area for placement of the tungsten recording electrode. During fLDI experiments, the scalp was retracted from the frontoparietal cortex by a dorsal midline incision to expose the cranium. The temporalis muscle was disconnected from the cranium and the skull area of $5 \times 5\,mm^2$ (2 mm posterior and 5 mm lateral to the bregma) enclosing the whisker barrel area on the left hemisphere was thinned to translucency using an air-cooled dental drill. During fMRI experiments, anesthetized and mechanically ventilated rats were placed in an animal holder with bite bars within the RF coil and magnet environment, and only the surgical procedures for placement of femoral catheters were performed.

Drug Treatments

Rats were grouped into three groups for each measurement modality. The first group was used for electrical recordings ($n = 14$), the second group for fMRI ($n = 10$), and the third group for fLDI measurements ($n = 13$). Within each measurement modality, rats were separated into Ru360 and Kaempferol drug treatment groups. Ru360 (EMD Biosciences, San Diego, CA, USA) working solution was prepared in physiologic saline and Kaempferol (Sigma Chemical Company, St Louis, MO, USA) working solution was prepared in physiologic saline with 20% dimethyl sulfoxide. Measurement after treatment with vehicle (20% dimethyl sulfoxide in saline) was performed in three rats in the fLDI measurement group to ascertain any dimethyl sulfoxide effects.

Rationale for the intravenous Ru360 dose ranges in this study was based on *in vivo* concentrations of Ru360 (15 to 25 μmol/L) that have been shown to depress the contractile force development in perfused heart.[29] Additionally, in our prior studies on the brain, we have characterized a wide dose range of Ru360 (40 to 360 μg/kg) and determined that Ru360 delivered intravenously in the 120 μg/kg range produced equivalent decreases in the stimulus-evoked fLDI activation area observed with a cerebrospinal fluid dose of 10 to 20 μg/kg,[40] similar to the dose levels that produced measurable physiologic effects in perfused heart.[29] With regards to Kaempferol, μM concentration of the drug has been shown to be protective against ischemia/reperfusion-induced damage in the rat brain.[41] Pharmacokinetic parameters after an intravenous administration of 25 mg/kg Kaempferol in rats indicate concentrations of up to 30 μM in the blood plasma.[42] Hence, Kaempferol doses approximating levels that conferred ischemic protection were used. In every animal, measurements were made before administration of the drugs or vehicle acted as control data points. Measurements were repeated after infusion of vehicle or drugs for the treatment data points. Depending on the drug treatment group, animals were infused with intravenous doses of 120 to 240 μg/kg Ru360 or with intravenous doses of 1 to 3 mg/kg Kaempferol. After drug infusion, a delay of 30 minutes was allowed before starting the acquisition of data.

Somatosensory Stimulation

As the somatosensory functional representation of the forepaw ($S1_{FL}$) is spatially smaller compared with the somatosensory barrel field ($S1_{BF}$), it was ideal for the single point electrical measurements. As hemodynamic responses are correlates of neuronal network activity, the relatively larger functional representation of $S1_{BF}$ provided maximum sensitivity to distinguish drug-induced differences in the spatial extent of the hemodynamic responses. Hence, forepaw stimulation was adopted for electrophysiology and whisker stimulation for the hemodynamic response mapping. The forepaw stimulus consisted of 2 mA amplitude electrical pulses of 0.3 msec duration delivered at 3 Hz. Stimulus was delivered in an ON-OFF pattern of 30 seconds prestimulus baseline followed by stimulation for 30 seconds followed by 30 seconds poststimulus baseline. For mechanical whisker stimulation, the right vibrissae were cut approximately 1.5 cm from the face to equalize their length in all rows. Trimmed whiskers were glued together with a masking tape to include rows (A to E) and arcs (1 to 4) of the whiskers including the straddlers β, γ, and δ that precede arc-1. Whisker deflection was carried out at 5 Hz frequency in the rostrocaudal direction using air puffs of 15 ms duration from a pressurized air source controlled through a solenoid (James Long Company, Caroga Lake, NY, USA) controlled by a A310 pulse generator (WPI instruments, Sarasota, FL, USA). Air puffs were delivered through plastic tubing connected to a standard 1 mL pipette tip that delivered the air puffs with enough velocity to deflect the tape binding the whiskers to approximately 0.5 cm. During fLDI measurements, whisker stimulation was delivered in an ON-OFF pattern with 40-second stimulation followed by 80-second periods of rest in three blocks. During fMRI measurements, whisker stimulation was delivered in an ON-OFF pattern of 30-second prestimulus baseline measurements followed by 30-second whisker deflection followed by 60-second poststimulus baseline.

Electrical Recording

A burr hole was drilled above the contralateral $S1_{FL}$ region and a high impedance (2 to 4 MΩ) tungsten electrode was inserted into the fourth cortical layer. Neural activity measurements in the form of multiunit activity (MUA) and local field potentials (LFP) were measured. Electrophysiological signals obtained were digitized at 20 kHz and filtered to LFP and MUA signals (Krohn-Hite, Brockton, MA, USA) by splitting the electrical signals into low (<150 Hz) and high frequency (0.4 to 10 kHz) bands using a Butterworth filter (24 dB per oct attenuation). Electrophysiological data were simultaneously recorded using the Spike2 software (Cambridge Electronic Design, Cambridge, UK).

Functional Magnetic Resonance Imaging

Functional magnetic resonance imaging acquisitions were performed using a modified 11.7T system with Varian (Agilent Technologies, Santa Clara, CA, USA) spectrometer and custom built ^1H surface coil (diameter 1.4 cm). Details of fMRI measurements are discussed elsewhere.[43,44] Briefly, BOLD signal was acquired with echo-planar imaging with sequential sampling[45] using gradient-echo contrast with the following parameters: repetition time (TR) = 1,000 ms; echo time (TE) = 16 ms; field of view $= 2.56 \times 2.56\,cm^2$; image matrix $= 64 \times 64$, number of repetitions (NR) = 120. Five contiguous coronal slices with 2 mm slice thickness were selected over the region +2 mm anterior to −6 mm posterior from the bregma point. Anatomic images were obtained using gradient echo multi slice or fast spin echo multi slice contrast sequences in 128×128 matrix and field of view $= 2.56\,cm^2$.

Functional Laser Doppler Imaging

A high resolution laser Doppler imaging scanner (Moor Instruments, Sussex, UK) was used for fLDI measurements. A set of plane mirrors in the device directed a beam of laser from a low power (2 mW ± 20%, 632.8 nm) He-Ne source onto the tissue surface and collected the scattered Doppler shifted beam from the tissue, which was focused onto a photo-detector. A mirror controlled by a motor enabled the laser beam to scan in a raster

pattern across the surface of the thinned skull and the laser Doppler flux signal (proportional to the tissue perfusion; CBF) at each measurement point was calculated and stored in pixels. Briefly, the distance between the scanner head and the thinned skull was 20 cm leading to an in-plane resolution of about $110 \times 110\,\mu m^2$ with fLDI images of 50×50 pixel matrix obtained covering a field of view of $5 \times 5\,mm^2$. Images were obtained over the contralateral cortex where the image field of view completely covered the thinned skull window. Images were obtained at a rate of 16 second per image and a dead time of 4 seconds between each image. Functional laser Doppler imaging scanning parameters were optimized for maximum microvascular specificity.[46]

Data Analysis

Neurophysiology. LFP and MUA time series were further processed to calculate the relative change of electrical signals in the prestimulus resting states or during the evoked stimuli.

Resting State Neural Activity. Prestimulus baseline data sections of 3-minute length were selected for analysis. Spike activity was extracted from MUA time series with wavelet spike sorting and superparamagnetic clustering algorithms. Spiking frequency was calculated in 1-second bins, and subsequently averaged in the selected time series. The LFP activity was estimated using the root-mean-square calculation. Briefly, the raw data were squared, averaged for 1-second bins, and the square root was calculated. Average root-mean-square was estimated for every data block.

Stimulation-Evoked Neural Activity. Data section with 90-second length containing 30-second prestimulus, 30-second stimulus and 30-second poststimulus continuous segments were considered for the stimulation-evoked neural activity analysis. Multiunit activity and local field potential activities were estimated using the root-mean-square calculation. The detailed description of the procedure is described earlier.[44] Briefly, the raw data were squared, averaged for 1-second consecutive bins, and the square roots of the averaged values were estimated. Note that this process created 1 Hz temporal resolution MUA and LFP time series with larger positive activity for the stimulated period, where the stimulus evoked responses were elevated from the prestimulus neural activities (Figure 3). The fractional change in response to evoked activation was estimated as the percent change in signal during the 'ON' period compared with the 'OFF' period of stimulation.

Functional Magnetic Resonance Imaging. All fMRI data were subjected to a translational movement criterion using a center-of-mass analysis. After masking of nonbrain tissues, the raw images were converted into binary maps (i.e., brain vs. background). Removal of image intensity information (i.e., binary maps) assured an unbiased analysis, not affected by stimulation-induced effects. For each binary map in the series two center-of-mass values were calculated, one for each in-plane direction. For all data sets, the deviation in the center-of-mass values in the series remained within 1/4 of a voxel. Hence, no data set were discarded due to motion concerns. Functional magnetic resonance imaging activation maps during whisker stimulation were generated using a *t*-test between the resting state and activated state image volumes using a threshold of $P < 0.05$ corrected for multiple comparisons. All activation maps were overlaid on the corresponding anatomic images. Single run data were used to create activation maps (30-second rest vs. 30-second stimulation). The time course of BOLD signals was generated from the significantly activated voxels.

fLDI. Functional laser Doppler images were analyzed using custom scripts in MATLAB (Natick, MA, USA) and AFNI software. Each fLDI experimental condition was repeated three times and the image data were concatenated to generate a time series of 75 two dimensional images. For determination of whisker activation-induced cortical activation, the fLDI signal time series from the experimental trials for each experimental condition were cross-correlated with a reference function similar to the timing of the whisker stimulus on a pixel-wise basis. Subsequently, the cross-correlation coefficients were used to detect task-activated pixels in the cortex. An uncorrected probability of $P \leqslant 0.05$ corresponding to a correlation coefficient value of 0.25 was used to threshold the activation maps. A cluster size of at least three contiguous pixels was subsequently used to control for false-positives. Statistical activation maps were overlaid on the respective baseline fLDI flux maps. Magnitude of fLDI flux change during different experimental conditions was estimated as the average percent change in fLDI flux from all activated pixels detected after cross correlationas described earlier.[46] As a control measure to ascertain any direct vascular effect of the drugs, mean baseline CBF levels for each experimental condition was estimated from the prestimulus baseline fLDI flux images. Cerebral blood flow level across each experimental condition in every animal was estimated by averaging the baseline fLDI flux across all pixels in the image field of view to determine the group average for each treatment condition.

Statistical significance between control and treated conditions were tested using a one-way analysis of variance with *post hoc* Tukey's HSD test. $P \leqslant 0.05$ was considered significant.

RESULTS

Ru360, a specific inhibitor of the mCU-mediated mitochondrial Ca^{2+} influx[6,26] and Kaempferol, a specific enhancer of the mCU-mediated mitochondrial Ca^{2+} influx[31–33] have no known specificity towards plasma membrane receptors or voltage-gated ion channels. Hence, they are most likely to influence mitochondrial function through an intracellular target. If the agents impacted spontaneous neural activity in the resting state (prestimulus baseline condition) after an intravenous administration, it would serve as a direct *in vivo* confirmation that Ru360 and Kaempferol entered cells including cortical neurons. To determine this, extracellular electrical recording from the somatosensory forelimb area ($S1_{FL}$) was performed in α-chloralose anesthetized rats before and after treatment with Ru360 or Kaempferol. Ru360 significantly diminished the resting state spiking frequency but not LFP signal (Figures 2A and 2B), while Kaempferol enhanced both the resting state spiking frequency and LFP activities (Figures 2C and 2D).

To ascertain mCU modulatory effects on evoked neuronal activity, sensory stimulation-evoked brain responses were measured during electrical forepaw stimulation from the $S1_{FL}$ region. Figures 3A-C show representative LFP and MUA traces during the control and Ru360-treated conditions. Change in electrical activity during stimulation from the prestimulus baseline levels were estimated over all animals from the group. The average percent change over nine rats in the MUA and LFP signals during the 'ON' and 'OFF' periods of the stimulus before and after Ru360 treatment are shown in Figures 3D and 3E, respectively. Ru360 treatment significantly decreased the stimulus-evoked MUA and LFP activities. In a different group of rats, sensory stimulation-evoked brain responses were measured before and after treatment with the mCU enhancer-Kaempferol. Figures 3F–H show the representative LFP and MUA traces during the control and Kaempferol treated conditions. The average percent change in MUA and LFP signal during the 'ON' and 'OFF' conditions of the forepaw stimulation before and after Kaempferol treatment in five rats are shown in Figures 3I and 3J respectively. Kaempferol increased MUA activity during the first dose thereafter which the increase saturated during the second dose (Figure 3I). LFP activity significantly increased during the second dose of Kaempferol (Figure 3J). Field potentials were attenuated every alternate stimulus at the stimulation frequency of 3Hz (Figure 3G). This variation in neural response was also observed in the Ru360 treated animals (Figure 3B) and was consistent with our previous observations using α-chloralose anesthesia.[44]

As mCU modulation directly impacted spontaneous and evoked neuronal activities, the effects on activity-induced hemodynamic responses sensitive to neurometabolic and neurovascular coupling were mapped using fMRI-BOLD and fLDI-CBF contrasts respectively. To maximize the sensitivity of detecting drug-induced differences in the spatial extents of the evoked activity-induced hemodynamic responses, the adjacent $S1_{BF}$having the largest spatial representation in rodents was also adopted. Whisker deflection led to reproducible BOLD activation in the contralateral $S1_{BF}$ region (Figure 4A; control). Stimulation-induced BOLD response amplitude and activation volume decreased in a

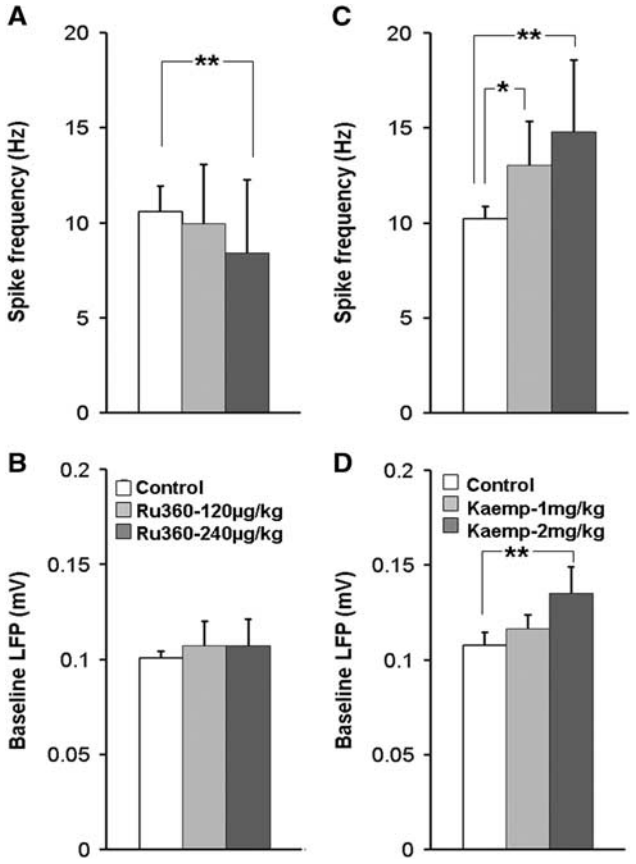

Figure 2. Calcium uniporter (mCU) modulation (inhibition or enhancement) impacted the resting state spontaneous cortical neuronal activity. Inhibition of mCU activity with Ru360 (dose-1 = 120 μg/kg; dose-2 = 240 μg/kg) significantly decreased (**A**) multi-unit (MUA) spiking frequency with no significant effect on (**B**) local field potential (LFP) amplitude. Significantly different during Ru360 treatment: $^{**}P \leqslant 0.05$; $^{*}P \leqslant 0.01$; one-way analysis of variance (ANOVA), *post hoc* Tukey's HSD test. Enhancement of mCU activity with Kaempferol (dose-1 = 1 mg/kg; dose-2 = 2 mg/kg) significantly increased (**C**) MUA spiking frequency with no significant effect on (**D**) LFP amplitude. Data represent 30 to 60 measurements across nine animals treated with Ru360 and five animals treated with Kaempferol. Significantly different, $^{**}P \leqslant 0.05$; one-way ANOVA, *post hoc* Tukey's HSD test.

Ru360 dose-dependent manner and was reproducible across animals (Figure 4A; 120 μg/kg and 240 μg/kg). Blood oxygen level dependant activation volume decreased significantly with Ru360 treatment over all rats within the group (Figure 4B). The average time course of the BOLD hemodynamic response decreased over all animals after Ru360 treatment (Figure 4C) with a significant dose-dependent reduction in the stimulation-evoked BOLD response magnitude (Figure 4D). Blood oxygen level dependant response amplitude and activation volume increased with the first dose of Kaempferol, which reverted back to control levels after administration of the second dose of Kaempferol (Figure 4E; 1 mg/kg and 2 mg/kg). Blood oxygen level activation volume increased significantly with the first dose of Kaempferol over all rats within the group (Figure 4F). No significant difference was observed in the BOLD activation volume after the second dose of Kaempferol compared with the control (Figure 4F). Figure 4G indicates the average time course of the BOLD hemodynamic response over all animals. From the group data, the first dose of Kaempferol significantly increased the stimulation-induced BOLD response but such an increase was absent during the second dose of Kaempferol (Figure 4H).

CBF responses were mapped over the contralateral $S1_{BF}$ region using fLDI in a separate group of rats. Whisker stimulation led to significant fLDI activations (Figure 5A; control). Functional laser Doppler imaging flux changes measured in the present configuration had a high specificity to microvascular CBF changes and were proximal to activated neural ensembles.[46] Multiple activation clusters well within the ($S1_{BF}$) area were detected with a good correspondence of the correlation coefficient values with activation-evoked changes in CBF (Figures 5A and 5B; control). Ru360 treatment led to a decrease in the spatial extent of fLDI activation in typical animals (Figure 5A; 120 μg/kg and 240 μg/kg). While the stimulation-evoked spatial extent decreased significantly over all animals (Figure 5C), the decrease in magnitude of the CBF change did not reach significance (Figure 5D). Kaempferol treatment led to an increase in the spatial extent of fLDI activation in typical animals (Figure 5E; 2 mg/kg and 3 mg/kg) and over all animals within the group (Figure 5G). However, the magnitude of the stimulation-evoked CBF change though increasing marginally, did not reach significance after Kaempferol treatment compared with vehicle (Figure 5H).

No peripheral physiologic effects of Ru360 and Kaempferol were apparent in the dose range used, as no significant drug-induced changes were observed in the mean arterial blood pressure, pH, or blood gases (Table 1). To ascertain any direct cerebvascular effects during drug treatment, prestimulus baseline CBF levels were measured before and after treatment with Ru360 or Kaempferol. No significant change was observed in the baseline CBF levels during treatment with both drugs (Figure 6). These results concur with our prior studies where a broader dose range of Ru360 treatment did not significantly impact the vascular reactivity in response to a transient hypercapnic stimulus.[40]

DISCUSSION

Ru360 has been shown to permeate cells *in vitro*,[26,47] depress the contractile force development, and elevate the resting tension in perfused heart.[29] Kaempferol (3,5,7-trihydroxy-2-(4-hydroxyphenyl)-4H-1-benzopyran-4-one), a natural flavonoid isolated from plant sources is a neuro and cardio protective agent. Kaempferol is transported into neurons in a concentration-dependent manner with minimal further metabolism[48] and blood micro molar concentrations protecting against ischemia/reperfusion-induced damage in the rat brain.[41] Pharmacokinetic parameters after intravenous administration of 25 mg/kg Kaempferol in rats indicate concentrations of up to 30 μM in the plasma.[42] The *in vivo* drug effects on evoked electrical activity and hemodynamic response demonstrated by the results along with prior evidence of a similar decrease in the spatial extent of activation-induced CBF response in the somatosensory cortex during intracerebroventricular, intravenous, or topical modes of delivery[40,49] suggest that Ru360 and Kaempferol may impact neuronal function and hemodynamic response through an intracellular target.

Neuronal and Hemodynamic Activity During Diminished Mitochondrial Ca^{2+} Uptake Capacity

During mCU inhibition, Ca^{2+} levels within cytoplasmic microdomains would swell *by* diffusion as they are no longer efficiently buffered. A swelling microdomain Ca^{2+} may lead to lesser Ca^{2+} mobilization from the endoplasmic reticular stores via diminished inositol-triphospate (IP_3) receptor activation in addition to a Ca^{2+}-dependent desensitization of the *N*-methyl *D*-aspartate subtype of the glutamate receptors, reducing further Ca^{2+} influx.[5,17,18] The resulting Ca^{2+} distribution in the different subcellular compartments during diminished mitochondrial Ca^{2+} uptake capacity (Figures 1B and 1E), would not only reduce oxidative energy metabolism via diminished mitochondrial Ca^{2+},[2,3] but

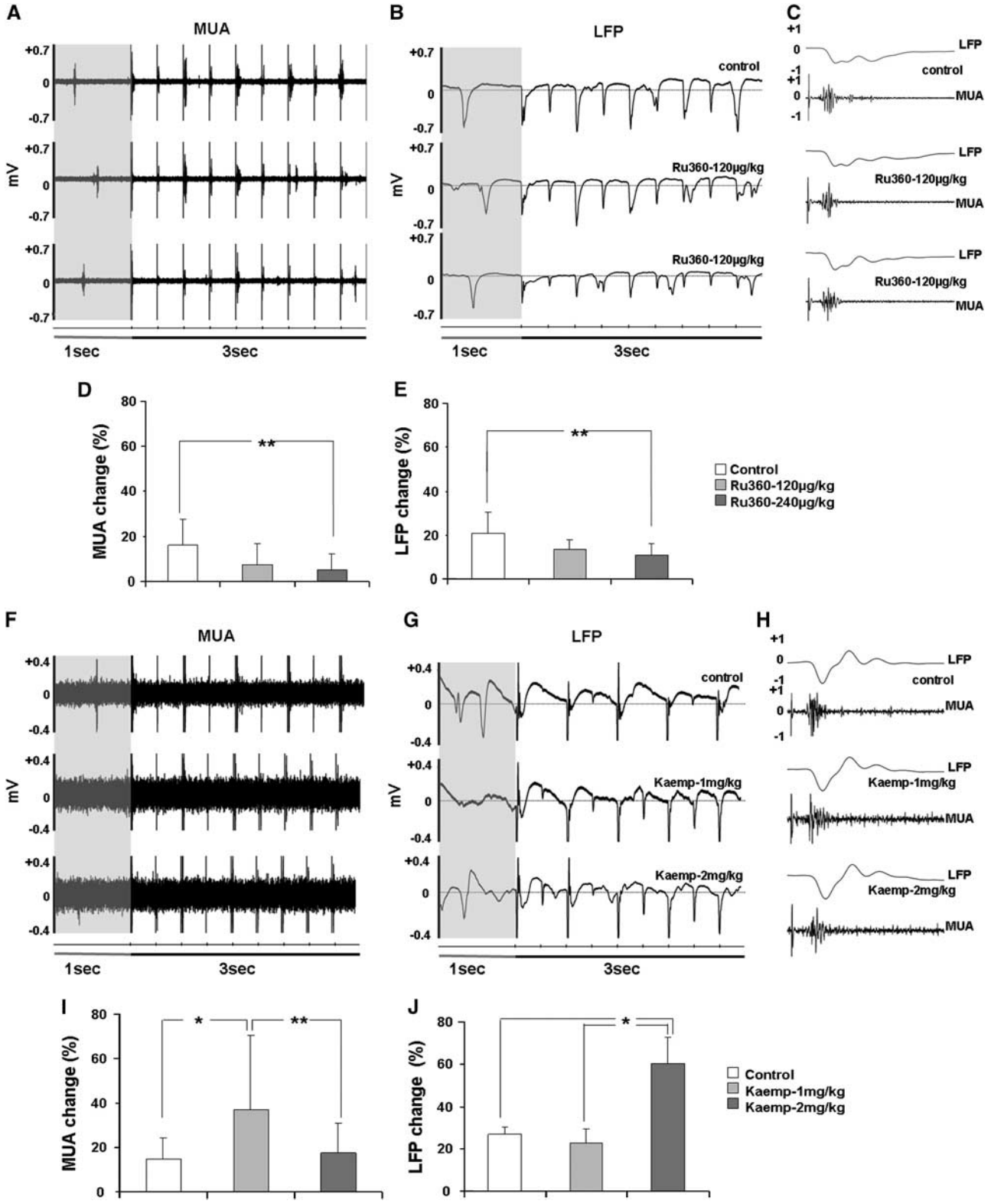

Figure 3. Representative traces of the forepaw stimulation-evoked electrical activity recorded from the contralateral $S1_{FL}$ region. (**A**–**C**) during Ru360 and (**F**–**H**) Kaempferol treatments in different time scales (prestimulus baseline indicated by the 1 second shaded interval in ((**A, B**) and (**F, G**)). Change in electrical activity (multiunit activity (MUA) and local field potentials (LFP)) during stimulation with respect to the prestimulus baseline levels estimated over all animals from the (**D, E**) Ru360 treated group (Ru360 dose-1 = 120 μg/kg; dose-2 = 240 μg/kg) and (**I, J**) Kaempferol treated group (Kaempferol dose-1 = 1 mg/kg; dose-2 = 2 mg/kg). Data represents mean ± s.d. from at least 50 measurements over nine rats in the Ru360 treatment group and at least 20 measurements over five rats in the Kaempferol treatment group. Significantly different, $^{**}P \leqslant 0.05$, $^{*}P \leqslant 0.01$; one-way analysis of variance, *post hoc* Tukey's HSD test.

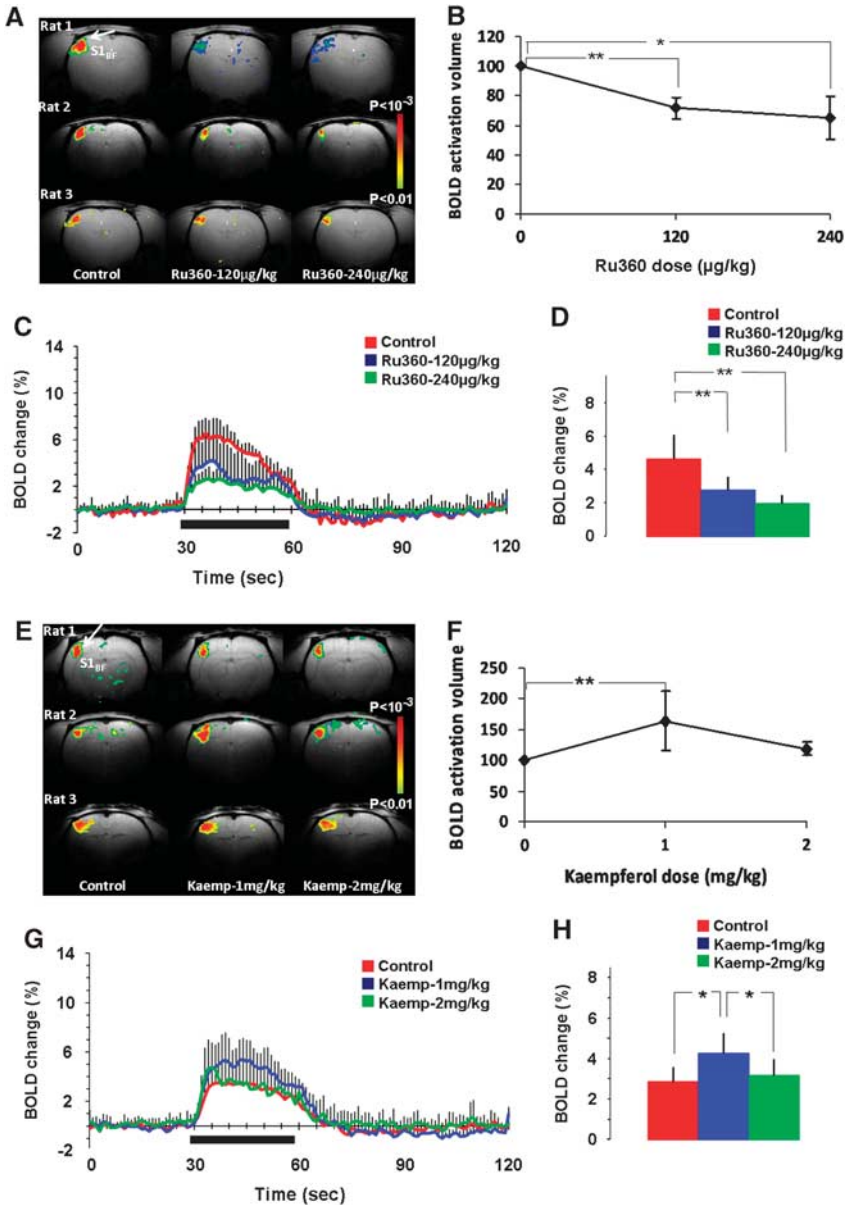

Figure 4. Dose dependent functional magnetic resonance imaging -blood oxygen level dependent (BOLD) responses to whisker stimulation in the (**A**–**D**) Ru360 (dose-1 = 120 μg/kg; dose-2 = 240 μg/kg) and (**E**–**H**) Kaempferol (dose-1 = 1 mg/kg; dose-2 = 2 mg/kg) treated rats. Whisker stimulation on the right side led to contralateral somatosensory barrel field activation ($S1_{BF}$; indicated by arrows). Ru360 in a dose dependent manner significantly decreased (**A**) BOLD activation volume in typical animals and (**B**) over all animals whereas Kaempferol in the lower dose increased (**E**) BOLD activation volume in typical animals and (**F**) over all animals. (**C**, **G**) averaged time course of the whisker stimulation-induced BOLD response from the statistically significant voxels in all animals in the Ru360 and Kaempferol treated groups, (**D**, **H**) time averaged BOLD response magnitude from the statistically significant voxels during the 30-second stimulation period from 15 trials over five rats each in the Ru360 and Kaempferol treated groups. Significantly different, $^{**}P \leqslant 0.05$; $^{*}P \leqslant 0.01$; one-way ANOVA, *post hoc* Tukey's HSD test.

additionally reduce neural activity through diminished Ca^{2+} influx into the cytoplasm.[5,23,30]

While diminished, unchanged, or increased overall cytoplasmic Ca^{2+} along with delayed recovery of the overall cytoplasmic Ca^{2+} have been observed *in vitro* during inhibited mitochondrial Ca^{2+} influx,[5,6,13,23] we hypothesized decreased cytoplasmic Ca^{2+} amidst an unchanged overall cytoplasmic Ca^{2+} (overall = cytoplasmic + microdomain) during mCU inhibition (Figures 1B and 1E) due to several reasons. Firstly, increased overall Ca^{2+} in many cellular studies demonstrated with the use of mitochondrial uncouplers should be cautiously interpreted due to concerns in the underlying bioenergetic states of the cells.[23] Secondly, optical microscopic measures of overall cytoplasmic Ca^{2+} at the single cell level can spatially exaggerate microdomain Ca^{2+} in the images, leading to an overestimation of actual cytoplasmic Ca^{2+} levels compounded further by swelling microdomain Ca^{2+} during inhibited mitochondrial Ca^{2+} uptake. *Ex vivo* studies of mitochondrial Ca^{2+} influx inhibition that avoid mitochondrial uncouplers and not focused on single cell level Ca^{2+} changes but population responses where these technical confounds are to a great extent mitigated, demonstrate decreased or no change in stimulus-evoked overall cytoplasmic Ca^{2+} responses.[5,13] The decreased spike rates in the spontaneously active neuronal networks (Figure 2A), a sensitive measure of diminished cellular signaling and mitochondrial oxidative metabolism,[50] bolster our hypothesis of a reduced mitochondrial and cytoplasmic Ca^{2+}

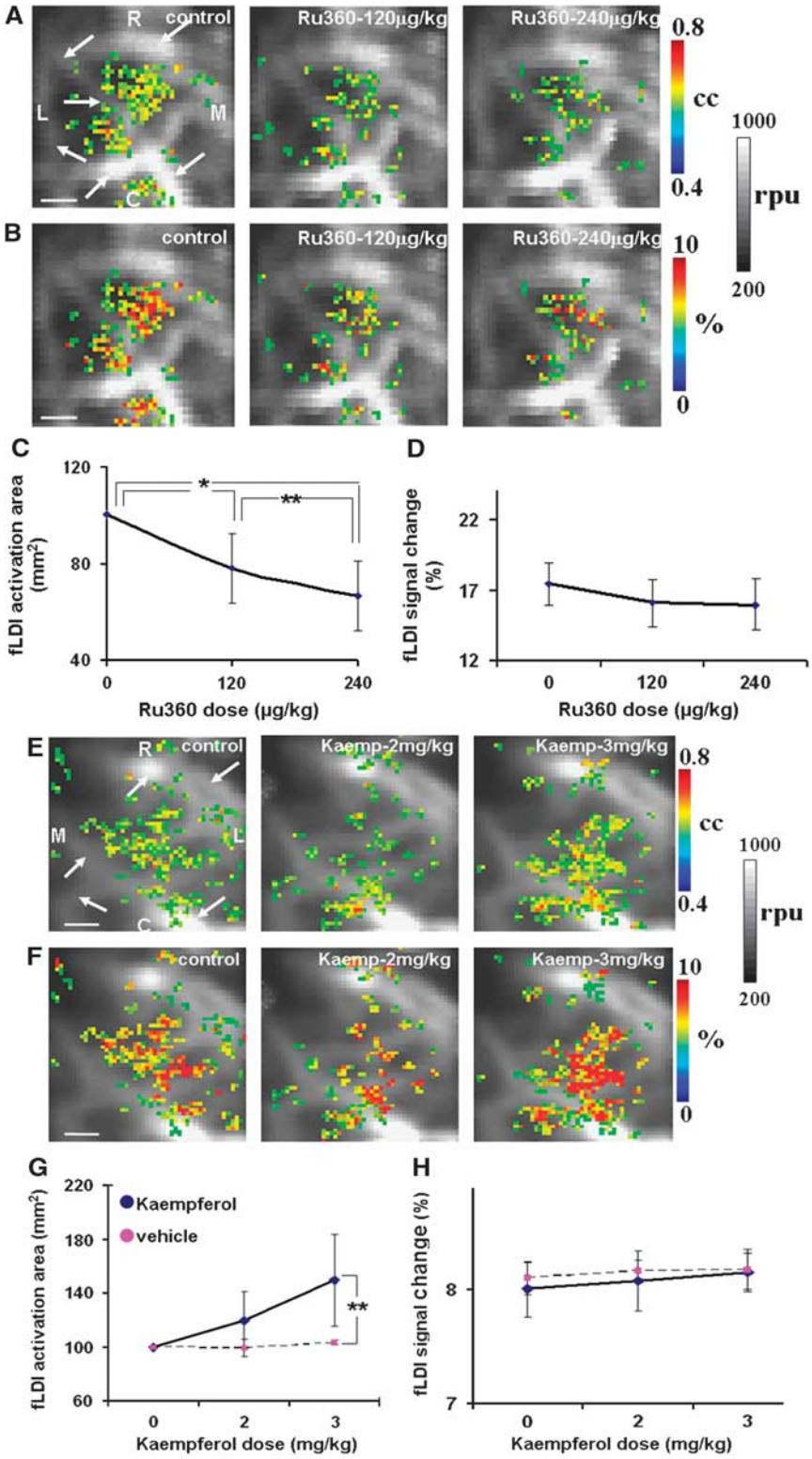

Figure 5. Representative contralateral $S1_{BF}$ activations (color-coded CBF changes) in response to whisker stimulation overlaid on the prestimulus baseline functional laser Doppler imaging flux images (gray scale in relative perfusion units-rpu). Large vessels with flux range 700 rpu and above are apparent in the baseline images (indicated by arrows). (**A**, **B**) representative activations during Ru360 treatment (dose-1 = 120 μg/kg; dose-2 = 240 μg/kg), (**E**, **F**) representative activations during Kaempferol treatment (dose-1 = 2 mg/kg; dose-2 = 3 mg/kg). Activated pixels color coded in (**A**, **E**) indicate correlation coefficients (cc) with a statistical threshold cc $\geqslant$ 0.23; equivalent to $P \leqslant 0.05$. Activated pixels color coded in (**B**, **F**) indicate fractional (cerebral blood flow) CBF change (%) within the activated pixels. Ru360 treatment significantly decreased (**C**) spatial extent of CBF response with no significant effect on (**D**) CBF magnitude. Kaempferol increased (**G**) spatial extent of CBF response with no significant effect on (**H**) CBF magnitude. Data represent mean ± s.d. from five rats each in the Ru360 and Kaempferol groups and three rats from the vehicle group. Significantly different, $^{**}P \leqslant 0.05$; $^{*}P \leqslant 0.01$; one-way analysis of variance, *post hoc* Tukey's HSD test. Scale bar = 1mm, R-rostral, M-medial, C-caudal and L-lateral.

Table 1. Vital physiologic parameters of the anesthetized animals before and after treatment with Ru360 and Kaempferol

	Urethane anesthesia				*α-Chloralose anesthesia*			
	MABP	*pH*	*pCO2*	*pO2*	*MABP*	*pH*	*pCO2*	*pO2*
Control	99 ± 8 (23)	7.33 ± 0.1 (14)	35 ± 8 (14)	148 ± 38 (14)	101 ± 11 (13)	7.34 ± 0.09 (12)	34 ± 6 (12)	141 ± 33 (12)
Ru360-1	98 ± 7 (12)	7.34 ± 0.06 (7)	39 ± 6 (7)	153 ± 37 (7)	101 ± 9 (7)	7.37 ± 0.04 (7)	37 ± 6 (7)	153 ± 20 (7)
Ru360-2	96 ± 7 (12)	7.37 ± 0.06 (7)	38 ± 7 (7)	156 ± 51 (7)	96 ± 9 (7)	7.33 ± 0.07 (7)	38 ± 4 (7)	148 ± 20 (7)
Kaemp-1	102 ± 11 (11)	7.36 ± 0.1 (7)	38 ± 6 (7)	139 ± 38 (7)	103 ± 8 (5)	7.35 ± 0.04 (5)	34 ± 5 (5)	137 ± 26 (5)
Kaemp-2	104 ± 10 (11)	7.33 ± 0.8 (7)	37 ± 7 (7)	133 ± 34 (7)	102 ± 10 (5)	7.43 ± 0.05 (5)	38 ± 6 (5)	134 ± 39 (5)

(Number of animals are indicated in parenthesis. MABP, mean arterial blood pressure.)

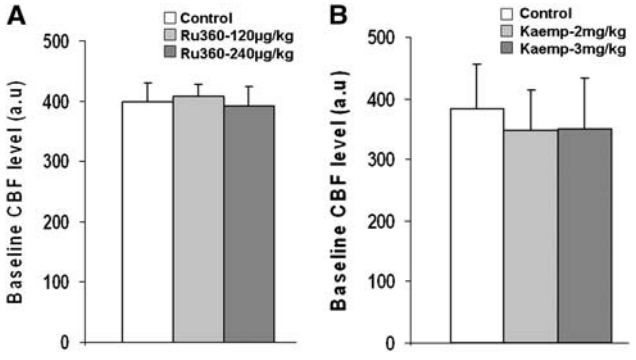

Figure 6. Inhibition of calcium uniporter (mCU) activity with Ru360 (dose-1 = 120 μg/kg; dose-2 = 240 μg/kg) had no significant effect on the (**A**) mean cerebral blood flow (CBF) level over five animals. Enhancement of the mCU activity with Kaempferol (dose-1 = 2 mg/kg; dose-2 = 3 mg/kg) also did not have any significant effect on the (**B**) mean CBF level over five animals.

influx within the constituent cellular populations leading to reduced oxidative metabolism and neuronal activity. A similar effect was observed during evoked activation (Figure 3). Even before a significant inhibition of activation-evoked MUA and LFP occurred (Figures 3D and 3E), BOLD (Figure 4D) and CBF responses (Figure 5C) were diminished during the first dose of Ru360 treatment. The diminished spatial extents in the BOLD and CBF responses indicate that diminished mitochondrial Ca^{2+} uptake capacities may also affect additional signaling mechanisms such as neuronal nitric oxide synthase activity. A reduced mitochondrial Ca^{2+} can diminish activation-induced production of nitric oxide that may contribute to diminish the activation-induced BOLD and CBF responses.[51]

Stimulus-evoked BOLD and CBF magnitudes were impacted differently during mCU inhibition with a 50% decrease in BOLD (Figure 4D) and no significant change in CBF (Figure 5D). The activation-evoked neuronal activity decrease (Figures 3D and 3E) with no significant effects on the stimulus-evoked CBF magnitudes (Figure 5D) suggest unique relationships between neuronal activity and magnitude of the relevant hemodynamic measures (whether CBF or BOLD).[52] Blood oxygen level dependent activity has been observed to change more rapidly than neuronal responses for small neuronal activity changes,[53] but very different for CBF (measured using laser Doppler). Unlike BOLD, CBF does not change till a threshold of neuronal activity is reached thereafter which, it changes in proportion to neuronal activity.[54] Based on the 50% reduction of the BOLD magnitude (Figure 4D), along with an intact coupling between MUA and LFP (Figures 3D and 3E), the difference between neural-BOLD and neural-CBF coupling seems to be widened during mCU inhibition. Furthermore, a sparse decrease observed in the spontaneous spiking frequency with no significant LFP change during mCU inhibition (Figures 2A and 2B) was accompanied by an unaffected baseline CBF level (Figure 6A). Extending the same argument from the evoked activity states[52–54] to the spontaneous state, the mCU inhibition-induced reduction in neuronal activity may not have been sufficient enough to sensitively detect any baseline CBF change. These relationships have implications in not only accurately interpreting task-induced changes in fMRI-BOLD and CBF contrast but also intrinsic activity of the brain using resting state fMRI.

Neuronal and Hemodynamic Activity During Enhanced Mitochondrial Ca^{2+} Uptake Capacity

Robust mitochondrial Ca^{2+} cycling during enhanced mCU activity may lead to lesser cytoplasmic microdomain Ca^{2+} due to enhanced Ca^{2+} uptake by mitochondria (Figures 1C and 1F). Owing to lesser microdomain Ca^{2+} accumulation, prolonged *N*-methyl *D*-aspartate receptor[17,18] and voltage-gated Ca^{2+} channel activity[16] may not only lead to a net increase in cytoplasmic Ca^{2+} influx but also increase subsequent mitochondrial Ca^{2+} cycling into the cytoplasm through the Na^{+}-Ca^{2+} and H^{+}-Ca^{2+} exchangers. Hence, a relatively larger overall cytoplasmic Ca^{2+} may augment energy metabolism, neuronal activity, and the collective excitability of the cortex. The results during mCU enhancement confirm our hypothesis where a significant increase in both spontaneous (Figures 2C and 2D) and stimulus-evoked neuronal activity change (Figures 3I and 3J) was observed. The stimulus-evoked changes in LFP and MUA were also uncoupled during Kaempferol treatment. With increasing doses of Kaempferol, the observed drug-induced increase in prestimulus baseline spontaneous spiking frequency (Figure 2C) would tend to lower any difference (percent change) in stimulus-evoked spiking frequencies. This was evident during the higher dose of Kaempferol where the prestimulus spontaneous spiking frequency increased by almost 40% (Figure 2C) leading to a significant attenuation of the stimulus-evoked spiking frequency change at the higher dose of Kaempferol (Figure 3G). The higher dose of Kaempferol may have sufficiently increased the baseline neuronal activity leading to increased baseline oxidative metabolism to affect cerebral metabolic rate of oxygen consumption ($CMRO_2$). As an increasing $CMRO_2$ component tends to diminish BOLD magnitude, the higher dose of Kaempferol is very likely to have increased activation-induced oxidative metabolism sufficiently to abolish the BOLD increase in magnitude and spatial extent (Figures 4F and 4H). Despite a relatively large increase in spontaneous neuronal activity during mCU enhancement (Figures 2C and 2D), baseline CBF levels were not significantly affected (Figure 6B). There is again the possibility that CBF may not be impacted till a threshold of spontaneous neuronal activity increase occurred.[52–54]

As the drugs were administered intravenously, general state changes can occur because secondary effects of the drug can possibly modify inputs to the cortical network. However, as the LFP and MUA responses were disassociated only during mCU enhancement (Figures 3I and 3J) without any treatment-induced

changes in the baseline CBF (Figure 6B), this effect cannot be solely attributed to any modified inputs to the cortical network or general state changes. To what extent neuronal activity couples to the LFP and to BOLD signal responses is significant to understand brain function and is still under debate. Spike and gamma-LFP power coupling can vary with time within a neuronal network and the extent of the coupling is linked to the degree of spike correlations between neighboring neurons.[55] For most situations, LFP maybe considered to be a good indicator of BOLD during either MUA-LFP correlated or dissociated conditions.[56] As evidenced by our results, BOLD signal was a better indicator of the MUA while CBF was a better indicator of LFP during Kaempferol treatment. The interesting correspondence of BOLD with MUA and CBF with LFP during the enhanced metabolic state along with dissociated MUA-LFP suggests the influence of the baseline metabolic state in not only determining neuronal synchrony within the network but also the way neural activity couples to either BOLD or CBF. Such a kind of altered MUA-LFP-hemodynamic relationship may signify altered cortical processing patterns.[57]

Potential Glial and Vascular Cell Contribution to the Modulated Brain Responses

As both drugs were applied systemically and do not specifically target cell types or receptors, the observed impact on the brain response is a cumulative effect from the neuronal, glial, and vascular compartments. However, neurons contain the largest mitochondrial density compared with other cell types in the brain with further higher concentrations of mitochondria in neuronal dendrites compared with cell body or axons. As the overall cytoplasmic Ca^{2+} from the brain tissue co-varies with the BOLD signal during evoked activation with the strongest correlation with neuronal Ca^{2+},[58] the observed systemic impact of Ca^{2+}-induced changes in electrical activities and hemodynamic responses may predominantly emerge from neuronal populations. Furthermore, astrocytic oxidative demand is approximately 20% of neuronal oxidative demand over a wide range of activities.[59–62] Thus, oxidative energy consumption in astrocytes can be considered less contributive than neurons to the observed effects. Therefore, the mCU inhibition-mediated decreases in brain activity may predominantly act through neuronal cell populations. However, the role of astrocytes in diminishing the activation-induced neuronal activity and spatial extents of the hemodynamic response cannot be completely ruled out as altered Ca^{2+} homeostasis in astrocytic populations may have a secondary impact on neuronal activities and BOLD signals.[8,21,58] Direct vascular impact of Ru360 was not apparent, as no significant effect was observed on the baseline CBF levels during treatment with Ru360 (Figure 6A). These results concur with our prior studies where a broader dose range of Ru360 treatment did not change the vascular reactivity to a transient hypercapnic stimulus in anesthetized animals.[40] Hence, in summary, the neural (neuronal and glial) compartment may contribute to the mCU inhibition-induced decreases in the cortical electrical and hemodynamic responses.

Direct vascular impact of Kaempferol treatment was not apparent as no significant effect was observed on the baseline CBF levels during treatment with both doses of Kaempferol (Figure 6B). Furthermore, Kaempferol dose-dependent increase followed by a return to normal in the BOLD spatial extent and magnitude (Figures 4F and 4H) was accompanied by a monotonic increase in CBF spatial extent (Figure 5G) and stimulation-evoked LFP change (Figure 3J). As CBF, $CMRO_2$ and cerebral blood volume (CBV) constitute the physiologic components of the BOLD signal, a substantially enhanced $CMRO_2$ component during the second dose of Kaempferol seems to saturate BOLD while CBF extents increased further. Increased electrical activity along with larger cytoplasmic and mitochondrial Ca^{2+} loads during mCU enhancement would help stimulate mitochondrial dehydrogenases,[2,3] higher reduction rate of NAD^+, increased lactate-pyruvate ratio, and higher aerobic glycolysis due to increased glial clearance of neurotransmitters.[59] Hence, strong neuronal (and glial) metabolic response may contribute to continuously enhance CBF while saturating BOLD. These results qualitatively support enhanced resting state spontaneous and evoked activity-dependent increase in oxidative demand and quantitatively support the recruitment of a larger network of neural populations (both neuronal and glial) during mCU enhancement.

Implications of Mitochondrial Ca^{2+} Uptake Imbalance in Neuropathology

Impact of mCU inhibition show similarities to hemodynamic and metabolic responses observed in normal aging humans and age-related neuropathologies. The evidence lead to the interesting hypothesis that reduced mitochondrial Ca^{2+} influx and cycling in aging humans may significantly diminish task-related neural activity and BOLD-fMRI response magnitudes more profoundly than task-related CBF response magnitudes. Positron emission tomography , fMRI, and magnetic resonance spectroscopic studies of normally aged humans indicate mitochondrial functional changes along with diminished baseline $CMRO_2$.[63–65] Assuming no age-related changes in neurometabolic coupling, the significantly larger evoked CBF as opposed to BOLD signal observed in older humans may be easily misinterpreted as evidence of an age-related increase in neural activity as cautioned by Restom *et al*,.[64] Our results during the mCU inhibited state that paralleled age-related decreases in mitochondrial oxidative metabolism show a greater ΔCBF compared with ΔBOLD accompanied by decreased neuronal activity. As diminished mitochondrial function is strongly implicated in human aging and age-related neuropathologies,[9,10,66,67] decreased mitochondrial Ca^{2+} uptake capacities may modulate activation-induced ΔCBF and ΔBOLD responses differently in humans. Thus, mitochondrial dysfunction with possible changes in neurometabolic coupling should be considered for an accurate interpretation of neuronal activity changes accompanying age-related task-fMRI-BOLD and CBF responses. Additionally fMRI, positron emission tomography, and magnetic resonance spectroscopic studies of penumbral tissue in the sub-acute stages after ischemia show enhanced neuronal activity accompanied by hypermetabolism.[11,12,68–71] As our multimodal evidence during mCU enhancement parallel neuronal and hemodynamic responses observed in acute stages of brain trauma,[69,72] the results raise an interesting hypothesis that enhanced mitochondrial Ca^{2+} influx and cycling in acute neuropathological states uncouple MUA and LFP activities and patently alter processing in cortical networks. As neuronal populations become hyperexcitable via enhanced mitochondrial Ca^{2+} influx and cycling, probabilities of epileptic seizures become greater during acute and subacute brain trauma.

CONCLUSION

The results provide evidence of mitochondrial Ca^{2+} uptake capacity to impact both spontaneous and evoked neocortical neuronal activities. Inhibition or enhancement of the mCU led to a decrease or increase in neuronal activity and activation-induced hemodynamic responses respectively. Deficient mitochondrial activities are indicated in chronic human neuropathologies such as aging and age-related neurodegenerative diseases whereas hyperactive mitochondrial activity and ionic stress are implicated in acute conditions after traumatic brain injury.[10] Hence, mitochondria *in vivo* can be viable drug targets to favorably

modulate (increase or decrease) neuronal and hemodynamic activities in human neuropathology.

DISCLOSURE/CONFLICT OF INTEREST

The authors declare no conflict of interest.

ACKNOWLEDGEMENTS

The authors thank Bei Wang for surgical and other colleagues at MRRC (mrrc.yale.edu) and Core Center for QNMR (qnmr.yale.edu) for technical assistance with the MR experiments. Critical inputs and suggestions from the anonymous reviewers have significantly improved the quality of this study and are gratefully acknowledged.

REFERENCES

1 Simpson PB. The local control of cytosolic Ca2+ as a propagator of CNS communication--integration of mitochondrial transport mechanisms and cellular responses. *J Bioenerg Biomembr* 2000; **32**: 5–13.
2 Duchen MR. Ca(2+)-dependent changes in the mitochondrial energetics in single dissociated mouse sensory neurons. *Biochem J.* 1992; **283**(Pt 1): 41–50.
3 McCormack JG, Halestrap AP, Denton RM. Role of calcium ions in regulation of mammalian intramitochondrial metabolism. *Physiol Rev* 1990; **70**: 391–425.
4 Bindokas VP, Lee CC, Colmers WF, Miller RJ. Changes in mitochondrial function resulting from synaptic activity in the rat hippocampal slice. *J Neurosci* 1998; **18**: 4570–4587.
5 Kannurpatti SS, Joshi PG, Joshi NB. Calcium sequestering ability of mitochondria modulates influx of calcium through glutamate receptor channel. *Neurochem Res* 2000; **25**: 1527–1536.
6 Mann ZF, Duchen MR, Gale JE. Mitochondria modulate the spatio-temporal properties of intra- and intercellular Ca2+ signals in cochlear supporting cells. *Cell Calcium* 2009; **46**: 136–146.
7 Rizzuto R, Simpson AW, Brini M, Pozzan T. Rapid changes of mitochondrial Ca2+ revealed by specifically targeted recombinant aequorin. *Nature* 1992; **358**: 325–327.
8 Simpson PB, Russell JT. Role of mitochondrial Ca2+ regulation in neuronal and glial cell signalling. *Brain Res Brain Res Rev* 1998; **26**: 72–81.
9 Beal MF. Mitochondria take center stage in aging and neurodegeneration. *Ann Neurol* 2005; **58**: 495–505.
10 Soane L, Kahraman S, Kristian T, Fiskum G. Mechanisms of impaired mitochondrial energy metabolism in acute and chronic neurodegenerative disorders. *J Neurosci Res* 2007; **85**: 3407–3415.
11 Nemoto EM, Jungreis C, Larnard D, Kuwabara H, Horowitz M, Kassam A. Hyperthermia and hypermetabolism in focal cerebral ischemia. *Adv Exp Med Biol* 2005; **566**: 83–89.
12 Sarnat HB, Flores-Sarnat L, Hader W, Bello-Espinosa L. Mitochondrial "hypermetabolic" neurons in paediatric epileptic foci. *Can J Neurol Sci* 2011; **38**: 909–917.
13 Fluegge D, Moeller LM, Cichy A, Gorin M, Weth A, Veitinger S *et al.* Mitochondrial Ca(2+) mobilization is a key element in olfactory signaling. *Nat Neurosci* 2012; **15**: 754–762.
14 Hajnoczky G, Robb-Gaspers LD, Seitz MB, Thomas AP. Decoding of cytosolic calcium oscillations in the mitochondria. *Cell* 1995; **82**: 415–424.
15 Kann O, Schuchmann S, Buchheim K, Heinemann U. Coupling of neuronal activity and mitochondrial metabolism as revealed by NAD(P)H fluorescence signals in organotypic hippocampal slice cultures of the rat. *Neuroscience* 2003; **119**: 87–100.
16 Kreiner L, Lee A. Endogenous and exogenous Ca2+ buffers differentially modulate Ca2+-dependent inactivation of Ca(v)2.1 Ca2+ channels. *J Biol Chem* 2006; **281**: 4691–4698.
17 Legendre P, Rosenmund C, Westbrook GL. Inactivation of NMDA channels in cultured hippocampal neurons by intracellular calcium. *J Neurosci* 1993; **13**: 674–684.
18 Lieberman DN, Mody I. Regulation of NMDA channel function by endogenous Ca(2+)-dependent phosphatase. *Nature* 1994; **369**: 235–239.
19 Nicholls DG. Mitochondria and calcium signaling. *Cell Calcium* 2005; **38**: 311–317.
20 Regehr WG, Connor JA, Tank DW. Optical imaging of calcium accumulation in hippocampal pyramidal cells during synaptic activation. *Nature* 1989; **341**: 533–536.
21 Verkhratsky A, Rodriguez JJ, Parpura V. Calcium signalling in astroglia. *Mol Cell Endocrinol* 2012; **353**: 45–56.
22 Pivovarova NB, Andrews SB. Calcium-dependent mitochondrial function and dysfunction in neurons. *FEBS J.* 2010; **277**: 3622–3636.
23 Budd SL, Nicholls DG. A reevaluation of the role of mitochondria in neuronal Ca2+ homeostasis. *J Neurochem* 1996; **66**: 403–411.
24 Parekh AB. Ca2+ microdomains near plasma membrane Ca2+ channels: impact on cell function. *J Physiol* 2008; **586**: 3043–3054.
25 Berridge MJ. Calcium microdomains: organization and function. *Cell Calcium* 2006; **40**: 405–412.
26 Matlib MA, Zhou Z, Knight S, Ahmed S, Choi KM, Krause-Bauer J *et al.* Oxygen-bridged dinuclear ruthenium amine complex specifically inhibits Ca2+ uptake into mitochondria in vitro and in situ in single cardiac myocytes. *J Biol Chem* 1998; **273**: 10223–10231.
27 Burkeen JF, Womac AD, Earnest DJ, Zoran MJ. Mitochondrial calcium signaling mediates rhythmic extracellular ATP accumulation in suprachiasmatic nucleus astrocytes. *J Neurosci* 2011; **31**: 8432–8440.
28 Kovacs R, Kardos J, Heinemann U, Kann O. Mitochondrial calcium ion and membrane potential transients follow the pattern of epileptiform discharges in hippocampal slice cultures. *J Neurosci* 2005; **25**: 4260–4269.
29 de Jesus Garcia-Rivas G, Guerrero-Hernandez A, Guerrero-Serna G, Rodriguez-Zavala JS, Zazueta C. Inhibition of the mitochondrial calcium uniporter by the oxo-bridged dinuclear ruthenium amine complex (Ru360) prevents from irreversible injury in postischemic rat heart. *FEBS J* 2005; **272**: 3477–3488.
30 Hashitani H, Lang RJ, Suzuki H. Role of perinuclear mitochondria in the spatiotemporal dynamics of spontaneous Ca2+ waves in interstitial cells of Cajal-like cells of the rabbit urethra. *Br J Pharmacol* 2010; **161**: 680–694.
31 Sergeant GP, Bradley E, Thornbury KD, McHale NG, Hollywood MA. Role of mitochondria in modulation of spontaneous Ca2+ waves in freshly dispersed interstitial cells of Cajal from the rabbit urethra. *J Physiol* 2008; **586**(Pt 19): 4631–4642.
32 Vay L, Hernandez-Sanmiguel E, Santo-Domingo J, Lobaton CD, Moreno A, Montero M *et al.* Modulation of Ca(2+) release and Ca(2+) oscillations in HeLa cells and fibroblasts by mitochondrial Ca(2+) uniporter stimulation. *J Physiol* 2007; **580**(Pt 1): 39–49.
33 Montero M, Lobaton CD, Hernandez-Sanmiguel E, Santodomingo J, Vay L, Moreno A *et al.* Direct activation of the mitochondrial calcium uniporter by natural plant flavonoids. *Biochem J.* 2004; **384**(Pt 1): 19–24.
34 de la Fuente S, Fonteriz RI, Montero M, Alvarez J. Dynamics of mitochondrial [Ca(2+)] measured with the low-Ca(2+)-affinity dye rhod-5N. *Cell Calcium* 2012; **51**: 65–71.
35 Masamoto K, Fukuda M, Vazquez A, Kim SG. Dose-dependent effect of isoflurane on neurovascular coupling in rat cerebral cortex. *Eur J Neurosci* 2009; **30**: 242–250.
36 Lindauer U, Villringer A, Dirnagl U. Characterization of CBF response to somatosensory stimulation: model and influence of anesthetics. *Am J Physiol* 1993; **264** (4 Pt 2): H1223–H1228.
37 Ueki M, Mies G, Hossmann K. Effect of α-chloralose, halothane, pentobarbital and nitrous oxide anesthesia on metabolic coupling in somatosensory cortex of rat. *Acta Anaesthesiol Scand* 1992; **36**: 5.
38 Masamoto K, Kanno I. Anesthesia and the quantitative evaluation of neurovascular coupling. *J Cereb Blood Flow Metab* 2012; **32**: 1233–1247.
39 Huttunen JK, Grohn O, Penttonen M. Coupling between simultaneously recorded BOLD response and neuronal activity in the rat somatosensory cortex. *Neuroimage* 2008; **39**: 775–785.
40 Kannurpatti SS, Biswal BB. Mitochondrial Ca2+ uniporter blockers influence activation-induced CBF response in the rat somatosensory cortex. *J Cereb Blood Flow Metab* 2008; **28**: 772–785.
41 Lopez-Sanchez C, Martin-Romero FJ, Sun F, Luis L, Samhan-Arias AK, Garcia-Martinez V *et al.* Blood micromolar concentrations of kaempferol afford protection against ischemia/reperfusion-induced damage in rat brain. *Brain Res* 2007; **1182**: 123–137.
42 Barve A, Chen C, Hebbar V, Desiderio J, Saw CL, Kong AN. Metabolism, oral bioavailability, and pharmacokinetics of chemopreventive kaempferol in rats. *Biopharm Drug Dispos* 2009; **30**: 356–365.
43 Sanganahalli BG, Bailey CJ, Herman P, Hyder F. Tactile and nontactile sensory paradigms for fMRI and neurophysiologic studies in rodents. *Methods Mol Biol* 2009; **489**: 213–242.
44 Sanganahalli BG, Herman P, Blumenfeld H, Hyder F. Oxidative neuroenergetics in event-related paradigms. *J Neurosci* 2009; **29**: 1707–1718.
45 Hyder F, Rothman DL, Blamire AM. Image reconstruction of sequentially sampled echo-planar data. *Magn Reson Imaging* 1995; **13**: 97–103.
46 Kannurpatti SS, Biswal BB. Frequency tuning in the rat whisker barrel cortex revealed through RBC flux maps. *Brain Res* 2011; **1417**: 16–26.
47 Zazueta C, Sosa-Torres ME, Correa F, Garza-Ortiz A. Inhibitory properties of ruthenium amine complexes on mitochondrial calcium uptake. *J Bioenerg Biomembr* 1999; **31**: 551–557.
48 Liu R, Wang X, Zhao Y, Wang Z, Du L. The uptake behaviors of kaempferol and quercetin through rat primary cultured cortical neurons. *Biomed Chromatogr* 2006; **20**: 1178–1184.

49 Mathiesen C, Caesar K, Thomsen K, Hoogland TM, Witgen BM, Brazhe A *et al.* Activity-dependent increases in local oxygen consumption correlate with post-synaptic currents in the mouse cerebellum *in vivo*. *J Neurosci* 2011; **31**: 18327–18337.
50 Huchzermeyer C, Albus K, Gabriel HJ, Otahal J, Taubenberger N, Heinemann U *et al.* Gamma oscillations and spontaneous network activity in the hippocampus are highly sensitive to decreases in pO2 and concomitant changes in mitochondrial redox state. *J Neurosci* 2008; **28**: 1153–1162.
51 Attwell D, Buchan AM, Charpak S, Lauritzen M, Macvicar BA, Newman EA. Glial and neuronal control of brain blood flow. *Nature* 2010; **468**: 232–243.
52 Heeger DJ, Ress D. What does fMRI tell us about neuronal activity? *Nat Rev Neurosci* 2002; **3**: 142–151.
53 Logothetis NK, Pauls J, Augath M, Trinath T, Oeltermann A. Neurophysiological investigation of the basis of the fMRI signal. *Nature* 2001; **412**: 150–157.
54 Norup Nielsen A, Lauritzen M. Coupling and uncoupling of activity-dependent increases of neuronal activity and blood flow in rat somatosensory cortex. *J Physiol* 2001; **533**(Pt 3): 773–785.
55 Nir Y, Fisch L, Mukamel R, Gelbard-Sagiv H, Arieli A, Fried I *et al.* Coupling between neuronal firing rate, gamma LFP, and BOLD fMRI is related to interneuronal correlations. *Curr Biol* 2007; **17**: 1275–1285.
56 Rauch A, Rainer G, Logothetis NK. The effect of a serotonin-induced dissociation between spiking and perisynaptic activity on BOLD functional MRI. *Proc Natl Acad Sci USA.* 2008; **105**: 6759–6764.
57 Nemoto M, Hoshi Y, Sato C, Iguchi Y, Hashimoto I, Kohno E *et al.* Diversity of neural-hemodynamic relationships associated with differences in cortical processing during bilateral somatosensory activation in rats. *Neuroimage* 2012; **59**: 3325–3338.
58 Schulz K, Sydekum E, Krueppel R, Engelbrecht CJ, Schlegel F, Schroter A *et al.* Simultaneous BOLD fMRI and fiber-optic calcium recording in rat neocortex. *Nat Methods* 2012; **9**: 597–602.
59 Azarias G, Perreten H, Lengacher S, Poburko D, Demaurex N, Magistretti PJ *et al.* Glutamate transport decreases mitochondrial pH and modulates oxidative metabolism in astrocytes. *J Neurosci* 2011; **31**: 3550–3559.
60 Hyder F, Patel AB, Gjedde A, Rothman DL, Behar KL, Shulman RG. Neuronal-glial glucose oxidation and glutamatergic-GABAergic function. *J Cereb Blood Flow Metab* 2006; **26**: 865–877.
61 Hyder F, Rothman DL, Bennett MR. Cortical energy demands of signaling and nonsignaling components in brain are conserved across mammalian species and activity levels. *Proc Natl Acad Sci USA* 2013; **110**: 3549–3554.
62 Wong-Riley MT. Cytochrome oxidase: an endogenous metabolic marker for neuronal activity. *Trends Neurosci* 1989; **12**: 94–101.
63 Boumezbeur F, Mason GF, de Graaf RA, Behar KL, Cline GW, Shulman GI *et al.* Altered brain mitochondrial metabolism in healthy aging as assessed by *in vivo* magnetic resonance spectroscopy. *J Cereb Blood Flow Metab* 2010; **30**: 211–221.
64 Restom K, Bangen KJ, Bondi MW, Perthen JE, Liu TT. Cerebral blood flow and BOLD responses to a memory encoding task: a comparison between healthy young and elderly adults. *Neuroimage* 2007; **37**: 430–439.
65 Yamaguchi T, Kanno I, Uemura K, Shishido F, Inugami A, Ogawa T *et al.* Reduction in regional cerebral metabolic rate of oxygen during human aging.. *Stroke* 1986; **17**: 1220–1228.
66 Kim J, Moody JP, Edgerly CK, Bordiuk OL, Cormier K, Smith K *et al.* Mitochondrial loss, dysfunction and altered dynamics in Huntington's disease. *Hum Mol Genet* 2010; **19**: 3919–3935.
67 Moreira PI, Cardoso SM, Santos MS, Oliveira CR. The key role of mitochondria in Alzheimer's disease. *J Alzheimers Dis* 2006; **9**: 101–110.
68 Busche MA, Chen X, Henning HA, Reichwald J, Staufenbiel M, Sakmann B *et al.* Critical role of soluble amyloid-beta for early hippocampal hyperactivity in a mouse model of Alzheimer's disease. *Proc Natl Acad Sci USA* 2012; **109**: 8740–8745.
69 Ding MC, Wang Q, Lo EH, Stanley GB. Cortical excitation and inhibition following focal traumatic brain injury. *J Neurosci* 2011; **31**: 14085–14094.
70 Tsytsarev V, Maslov KI, Yao J, Parameswar AR, Demchenko AV, Wang LV. *In vivo* imaging of epileptic activity using 2-NBDG, a fluorescent deoxyglucose analog. *J Neurosci Methods* 2012; **203**: 136–140.
71 Zetterling M, Hallberg L, Hillered L, Karlsson T, Enblad P, Ronne Engstrom E. Brain energy metabolism in patients with spontaneous subarachnoid hemorrhage and global cerebral edema. *Neurosurgery* 2010; **66**: 1102–1110.
72 Slobounov SM, Zhang K, Pennell D, Ray W, Johnson B, Sebastianelli W. Functional abnormalities in normally appearing athletes following mild traumatic brain injury: a functional MRI study. *Exp Brain Res* 2010; **202**: 341–354.